ELSEVIER

Contents lists available at ScienceDirect

Journal of Constructional Steel Research

journal homepage: www.elsevier.com/locate/jcsr





Fatigue behaviour of toe crack at the lower end of crossbeam-to-stiffener weld with cut-outs in OBDs

Weijian Wu^a, Johan Maljaars ^{b,c}, David Malschaert ^{a,d,*}, Milan Veljkovic ^a, Henk Kolstein ^a, Richard Pijpers ^b

- a Delft University of Technology, Mekelweg 5, Delft, The Netherlands
- b TNO, Molengraaffsingel 8, Delft, The Netherlands
- ^c Eindhoven University of Technology, Blauwe Zaale 1, Eindhoven, The Netherlands
- d Iv, Noordhoek 37, Papendrecht, The Netherlands

ARTICLE INFO

Keywords: Orthotropic bridge deck Crossbeam-to-stiffener Cut-outs Hot spot stress Fatigue resistance Influence surface

ABSTRACT

Steel Orthotropic Bridge Decks (OBDs) are widely used in the superstructures of movable and long-span bridges. There is a high concentration of stress at many welded connections, which are governing the fatigue performance of OBDs. The fatigue behaviour of the lower end of weld in crossbeam-to-stiffener connection with cut-outs is studied from multiple experimental results obtained from a 48 m² full-scale specimen, as well as finite element simulations. The fatigue resistance of the detail is recommended based on 8 experiments reported in the current study and experiments in the literature using the hot spot stress method. The influence of the load position on the hot spot stress is analysed. The effective notch stress method is used to evaluate the fatigue resistance with different weld profiles.

1. Introduction

Steel Orthotropic Bridge Decks (OBDs) have been widely used in bridge engineering [1]. The all-welded structure is common in long-span and movable bridges due to its high load-carrying capacity, relatively low self-weight, and fast construction [2]. It can also be used to replace the deteriorated concrete decks [3]. In general, an OBD comprises a deck plate, supported by longitudinal stiffeners and crossbeams, and connected by welds, see Fig. 1. Traffic loads are transferred to the deck plate, and then to the stiffeners and crossbeams. There are open-shape stiffeners and closed-shape stiffeners in OBDs. Closed stiffeners are favourable where high torsional rigidity is beneficial [4]. For the convenience of fabrication, cut-outs in crossbeams, below stiffeners, are used with two types of shapes, Haibach-type or regular-type, as indicated in modern OBDs.

OBDs experience a large number of load cycles in service. Welded connections cause high stress concentrations [2,5]. Moreover, high residual stresses and initial flaws, caused by the manufacturing and/or fabrication, exist at welds. This combination makes welded OBD structures sensitive to fatigue. Fatigue cracks were reported or studied near or in welds including but not limited to: stiffener-to-deck plate welds, crossbeam-to-stiffener welds, crossbeam-to-deck plate welds, stiffener-to-stiffener welds, and deck plate-to-deck plate welds. The cracks may initiate from the weld toe (T) or weld root (R) and propagate into base metal or weld metal.

A typical type of crack initiates at the lower end of the weld between the stiffener web and crossbeam in connection with a cut-out. This crack initiates at the weld toe at the stiffener's side, and it propagates outside of the vicinity of the weld (designated as type C3a in prTS 1993-1-901 [7]), see Fig. 2. Stress ranges ($\Delta \sigma$) are introduced due to the local distortion of the stiffener below C3a in combination with the in-plane and out-of-plane deformation of the crossbeam, causing stress concentrations at the weld toe. This type of crack was observed in bridges in Europe [1,4], Japan [8], the United Sates [9], and China [10].

Detail C3a has been studied by researchers using experiments and Finite Element (FE) simulations [1,10–15]. A relatively slow crack propagation rate for this detail is attributed to the cracks growing away from the crossbeam weld with its stress-raising effect. The criterion, i.e. the crack size, at which the fatigue resistance is determined becomes relevant. Some of the mentioned studies used a certain surface crack length as the criterion. Others used the first time a crack was observed by the naked eye ("first visible crack"), which is accompanied by some scatter related to detectable crack length and inspection interval. As an early indicator of cracking, many authors considered a certain deviation in the strain range, measured by a strain gauge concerning the initial strain range of the intact specimen. However, a well-defined and widely accepted verification method is currently

^{*} Corresponding author at: Delft University of Technology, Mekelweg 5, Delft, The Netherlands. E-mail address: d.h.malschaert@tudelft.nl (D. Malschaert).

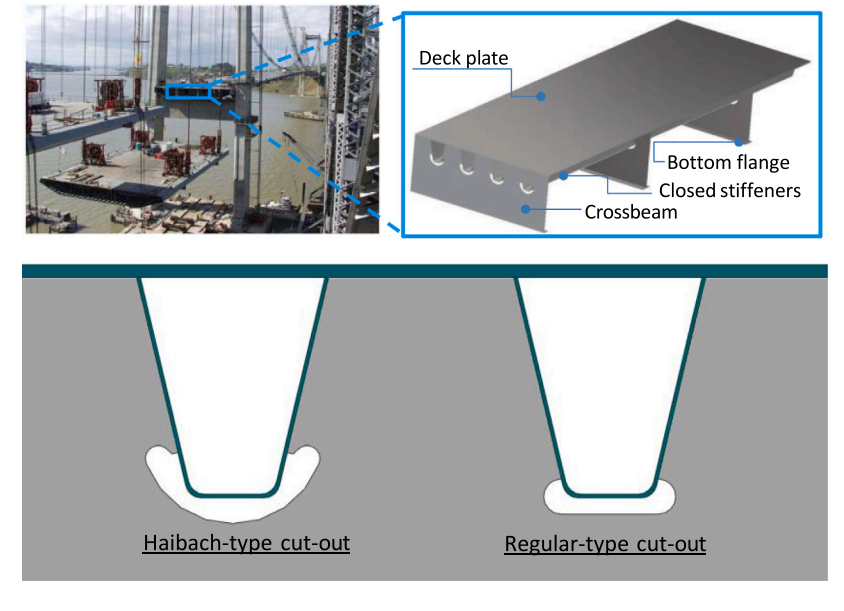
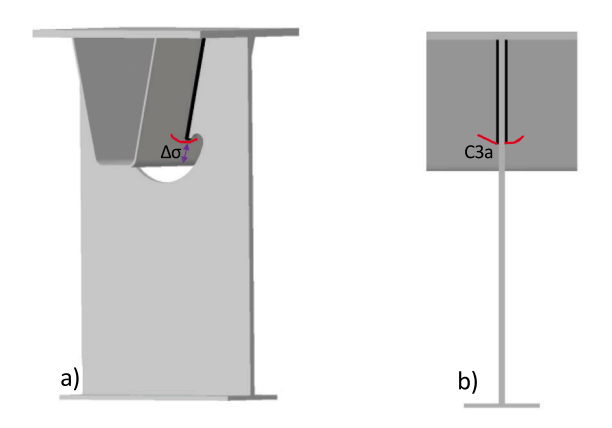


Fig. 1. Sketch of a representative modern OBD with cut-outs shapes commonly used in Europe [2,6].



 $\begin{tabular}{ll} Fig.~2. & Illustration of toe crack at the lower end of a crossbeam-to-stiffener weld with a cut-out. \end{tabular}$

missing. The detail was included by neither in the first nor in second generation of (pr)EN1993-1-9 [16,17].

This paper first experimentally studies the fatigue behaviour of detail C3a at eight locations in one full-scale specimen. The strain distribution is obtained by strain gauges, and surface cracks are tracked during the experiments. Subsequently, a FE model is described, which is validated using the measured strains. The Hot Spot Stress (HSS) is calculated using Finite Element Analysis (FEA). Afterwards, data from the current experiments and selected from the literature are grouped to derive a fatigue resistance that is proposed for the Technical Specification TS 1993-1-901 "Fatigue design of orthotropic bridge decks with the hot spot stress method" (TS in short). This TS will be part of the second generation of Eurocodes [7]. An additional S-N curve is proposed for existing brdige decks. The influence surface caused by the wheel loading is numerically investigated for the HSS of detail C3a. Finally, the Effective Notch Stress (ENS) method is adopted to study the effect of weld profiles.

2. Background of S-N curve

S-N curves are commonly used in high-cycle fatigue analysis. The Basquin relationship is employed for the number of cycles to failure

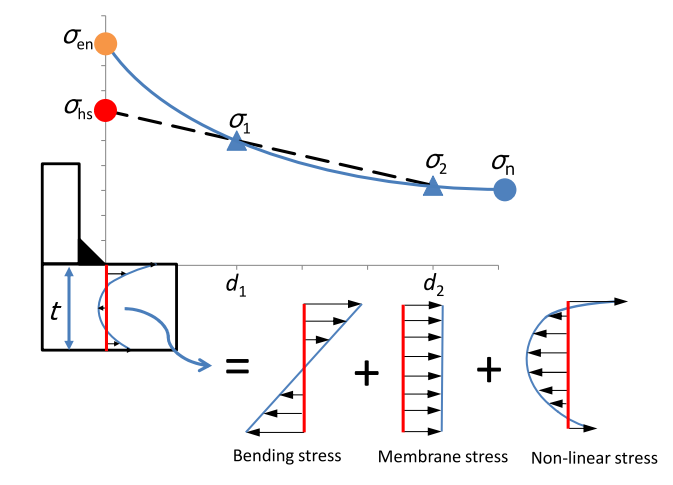


Fig. 3. Illustration of the stress path in a component in the vicinity of a weld.

 $N_{\rm R}$ as a function of the applied stress ranges $\Delta\sigma,$ as shown in Eq. (1).

$$log N_{\rm R} = a - m \cdot log \Delta \sigma \tag{1}$$

The slope parameter of S-N curve m and material constant a depend on the details and failure types. $\Delta \sigma_C$ is the stress range at which the 95% lower prediction bound of the number of cycles to failure is 2 million, assuming a fixed slope parameter of m = 3 or 5 [16,18]. A statistical analysis of the experimental data provides the values of a and $\Delta \sigma_C$.

The S-N curve is associated to the definition of stress used to derive it. Fig. 3 illustrates the stress path in a component in the vicinity of a weld. The Nominal Stress (NS), $\sigma_{\rm n}$, uses the stress in the base metal or in a weld calculated at the point of a potential crack location and all stress concentration effects already accounted for in the fatigue detail category. It is the main basis for fatigue design in standards and guidelines such as the European standard (pr)EN1993-1-9 [16,17], American AASHTO LRFD design specifications [19], and Japanese JSSC fatigue design recommendations [20]. Geometric stress concentrations are taken into consideration by the HSS, $\sigma_{\rm hs}$, which uses the stress in the base metal at the weld toe, incorporating all stress raising effects due to the overall detail geometry, but excluding that of the weld profile itself. $\sigma_{\rm hs}$ can be calculated by extrapolating the surface stress from

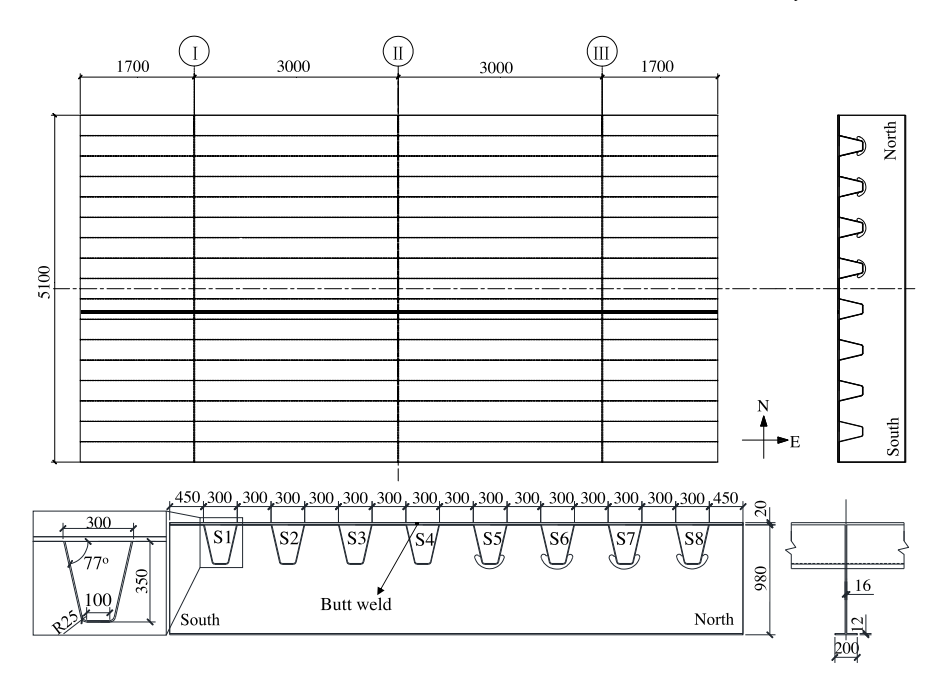


Fig. 4. Overview of the full-scale specimen (unit: mm) [6].

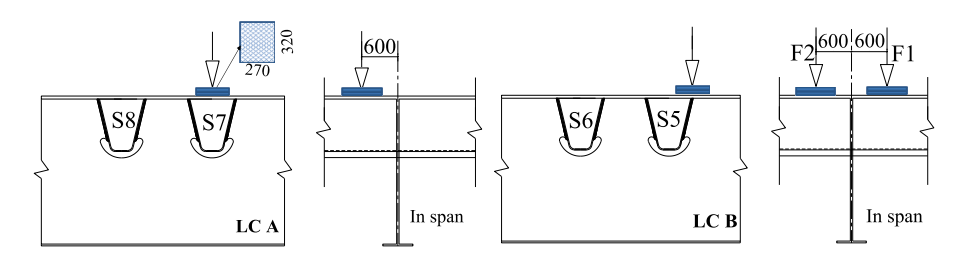


Fig. 5. Sketch of the out-of-plane loading positions for cross-beam-to-stiffener welds with Haibach type cut-outs (unit: mm).

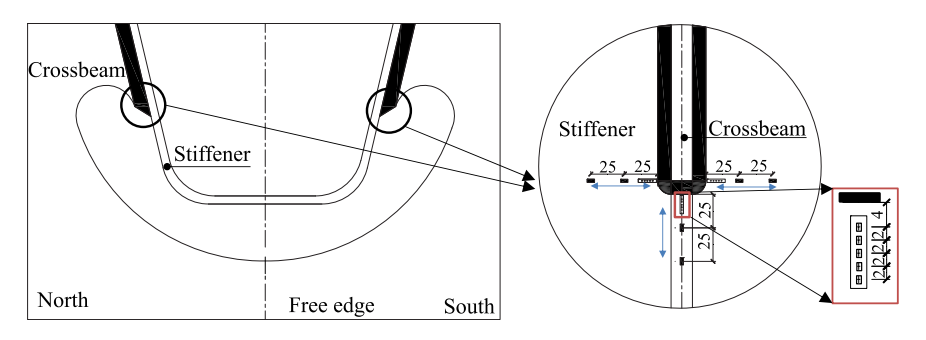


Fig. 6. Overview of the strain gauges positions at S5 to S8 (unit: mm).

predefined locations to the weld toe [7,21,22], or extracted from the traction forces at the studied cross-section [23]. The former is widely adopted in design guidelines and standards and has recently been used in OBDs [19,24–26]. The definition of HSS in the current paper follows the recommendation in TS [7], using the stress perpendicular to the weld toe at locations 0.5t and 1.5t away from the weld toe, where t is the thickness of the plate. The ENS, $\sigma_{\rm en}$, uses the total stress in a fictitious notch at the weld toe or root. It includes the effect of all geometric properties of the welded detail including the stress peak due to the weld itself, and resulting in locally varying stress distribution (nonlinear peak stress) [17,21,27,28]. Local geometric characteristics and stress states can be evaluated using $\sigma_{\rm en}$. Table 1 summaries $\Delta\sigma_{\rm C}$ used in the bridge standards and guidelines, with the AASHTO designation system [19] transferred to $\Delta\sigma_{\rm C}$.

 $\Delta \sigma_{\mathbb{C}}$ of welded steel plate connections in the bridge standards and guidelines.

Source	Method	Application	m	$\Delta\sigma_{C}$ [MPa]
[17,19,20]	NS	T & R	3 or 5	36 to 125
[17,19,20]	HSS	T	3	80 [20], 90 [17,19], 100 [17,20]
[17]	ENS	T & R	3	200 or 225

OBDs contain components of various plate thicknesses (6 mm to 24 mm) that experience complicated multi-axial stress states (bending and compression in many cases). Relative slow propagation is observed in some details. Recent studies show that welded connections in or at the deck plate can have fatigue resistances deviating from the values in Table 1 [6,29,30]. In addition to relative slow crack propagation, detail C3a experiences a large proportion of bending and has a relatively thin

plate (6 or 8 mm). It is noticed both by the experimental investigations and fracture mechanics calculations that bending stress is less detrimental than membrane stress [31,32]. In addition, steeper stress gradients exist in thinner plates. This may all result in a relatively higher fatigue resistance [31,33]. On the other hand, the detail is loaded in multiple directions, by the distortion of the stiffener and by in- and out-of-plane deformation of the crossbeam. It is therefore difficult to estimate its fatigue resistance without experiments specifically aimed at fatigue cracking of this detail.

3. Experimental investigation and FE model validation

3.1. Specimen description

Experiments are carried out using the full-scale specimen as shown in Fig. 4. The specimen is made from structural steel grade S355J2 with a nominal yield stress of 355 MPa [34]. The 20 mm thick deck plate is strengthened by 6 mm thick trapezoidal-shaped stiffeners. The 16 mm thick crossbeams web are connected to the stiffeners and deck plate by fillet welds. Extended cut-outs with the Haibach-type shape are used on the north side of the specimen, whereas the crossbeams are welded around the entire perimeter of the stiffeners (without cut-outs) on the south side. The latter are not the subject of the current study and are therefore not further mentioned. The crossbeam-to-stiffener welds are automatically welded by one pass. The Flux-Cored Arc Welding (FCAW) is used with DC+ type current. Fillet welds have an effective thickness of 5 mm. The welding parameters are: 1.2 mm wire diameter, 270 to 300 ampere current, 28 to 30 voltage, 23 to 31 cm/min speed, and 1.5 to 2.4 kJ/mm heat input. The welds comply with the quality level B of ISO 5871 [35].

3.2. Set-up and loading programme

Two series of load cases, LC A and LC B, are applied in the experiments, see Fig. 5. In LC A, the cyclic load is applied on the free edge side of crossbeam I with the loading patch centred above the stiffener. In LC B, cyclic loads F1 and F2 are simultaneously applied on the free edge and in span sides, with the load centred above a stiffener web. The load patch has a size of 270 mm × 320 mm, corresponding to the tyre patch of Axle Type C in EN1991-2 [36] with two layers of 8 mm thick rubber plates between the top of the deck plate and the steel load jack at each load application position. Naked eye inspections are carried out to detect surface cracks during the experiments. Table 2 gives a summary of the experimental programme. LC A is firstly applied on stiffeners 7 (S7) and 8 (S8) without cracks observed. Thereafter, LC B is applied, resulting in fatigue cracks at the detail of study. Note that S8 N has been loaded first in LC A, and then two strengthening plates (approximately 50 mm thick steel plates) are placed on the deck plate at the load application positions with a size of approximately 500 mm × 500 mm before LC B is applied. This strengthening is applied due to the fatigue cracks in the stiffener-to-deck plate weld (on the north side of S7) and base metal, both observed below the load patch after S7 L&R are loaded in LC A. As the stress levels of the stiffener-to-deck plate welds in LC B are significantly smaller than LC A, strengthening is not needed for LC B. Therefore, they are not used for S5 and S6. The following part of the paper focuses on the description of LC B. To obtain a conservative $\Delta\sigma_C$, the cycles loaded in LC A are not counted in the current paper.

3.3. Strain measurement

Fig. 6 gives an overview of the strain gauges attached to the stiffeners of S5, S6, S7, and S8. The strains in the horizontal directions and the direction perpendicular to the weld toe at the lower end are referred to as "Stiffener H1 (free edge)", "Stiffener H2 (in span)", and "Stiffener V", respectively. In each of these directions, a chain of 5 strain gauges with an intermediate distance of 2 mm is attached to cover the local

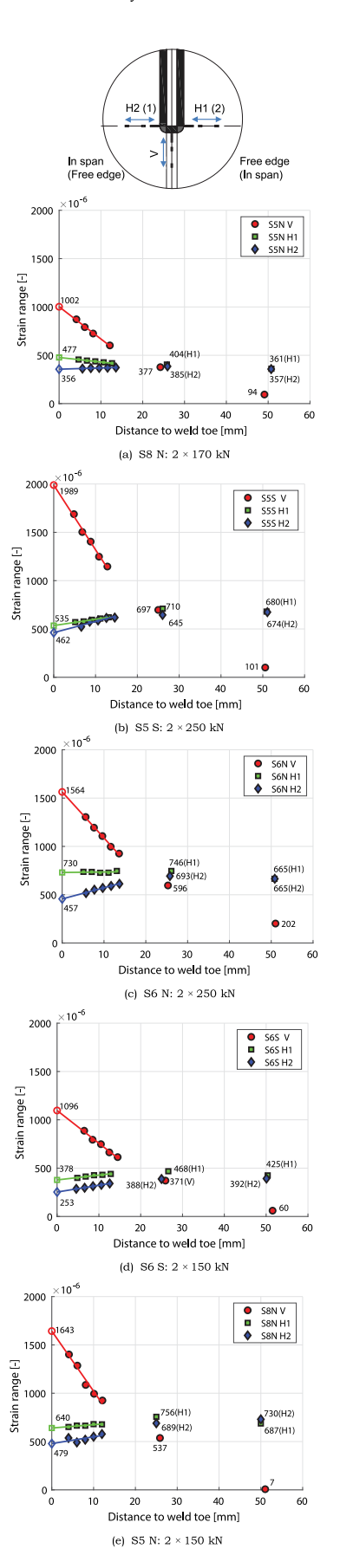


Fig. 7. Strain ranges close to the weld toe, measured in LC B.

Table 2
A summary of the loading programme

	Stiffener ID	7 S&N	7 S&N	7 S&N*	8 S&N*
	Load range [kN]	1 × 275	1 × 360	1 × 360	1 × 320
	Frequency [Hz]	2	2	2	2
LC A	Load ratio	0.1	0.1	0.1	0.1
	Cycles [million]	7.40	0.67	1.73	9.91
	Run-out	×	×	×	×

	Stiffener ID	8 N*	5 S	6 N	6 S	5 N
	Load range [kN]	2 × 170	2 × 250	2 × 250	2 × 150	2 × 150
	Frequency [Hz]	2	2	2	2	2
LC B	Load ratio	0.1	0.1	0.1	0.1	0.1
	Cycles [million]	0.33	0.31	0.55	1.67	10.00
	Run-out					×

Note:

[&]quot;x" run-out.

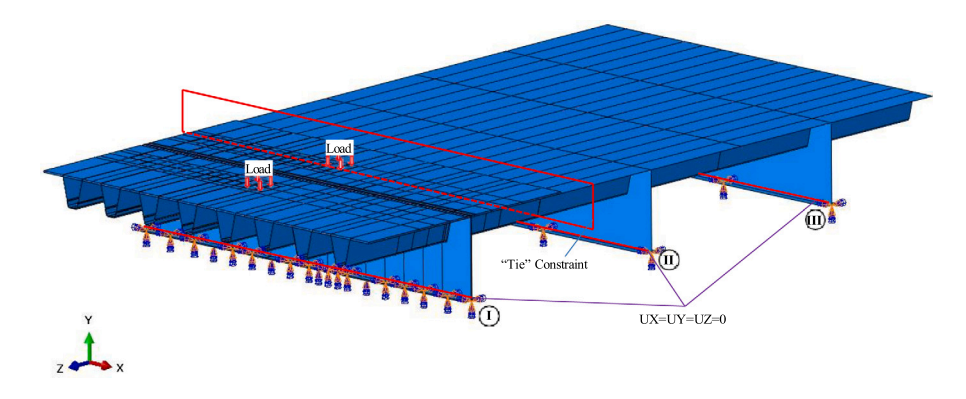


Fig. 8. Load and boundary conditions of the FE model.

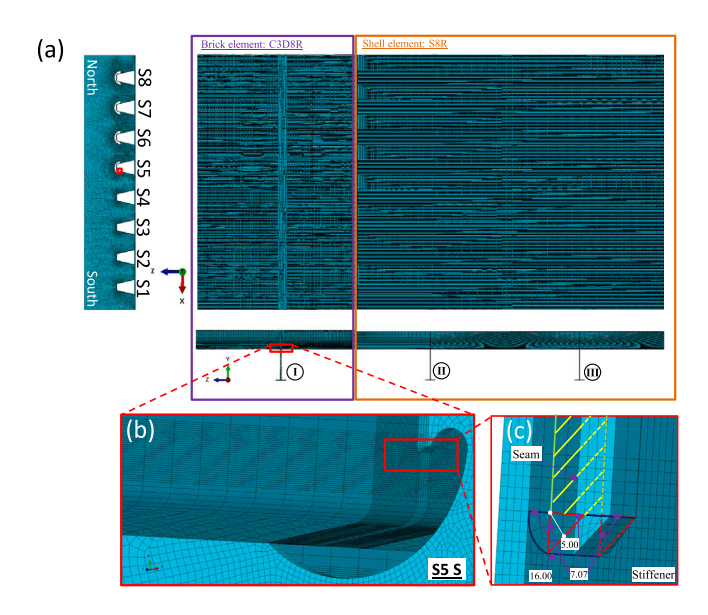


Fig. 9. FE model of the specimen and the lower end of the crossbeam-to-stiffener weld in S5 S (unit: mm).

stress field, with the first gauge intended to be positioned 4 mm from the weld toe. Stress gradients are obtained by the chain strain gauges, which can be used in the HSS calculations [21]. In addition, two separate gauges intended at 25 mm and 50 mm distances from the weld toe are attached to cover the global strain field.

Fig. 7 presents the measured strain ranges close to the weld toe. The positions of the strain gauges are measured after the experiments

and used in Fig. 7. One exception is S8 N, where the strain gauges are removed before executing measurements, the intended distances are therefore used for S8 N. The strains in Fig. 7 are positive in V direction and negative in H1 and H2 directions at the applied loads, although strain ranges are always positive. The highest strain ranges are observed at the lower end (V direction). The strain values in H1 and H2 directions are smaller than those in V direction. The ranges on the free edge side (H1) are slightly larger than those on the in span side (H2). High strain ranges and concentrations are observed in the V direction. The linear extrapolation is carried out using the 5 strain measurements close to the weld toe. The extrapolated strain ranges in H1 and H2 directions are between 2 and 4 times lower than the values in V direction.

3.4. Introduction of the FE model

Fig. 8 shows the FE model constructed using the commercial software Abaqus 2019 [37]. A uniform distributed pressure is applied to the load areas. Displacement constraints are applied along the centre lines of the crossbeams at the bottom flanges in three dimensions (UX=UY=UZ=0). The linear elastic material is applied in the model with the Elastic modulus $E_{\rm S}=210$ GPa and Poisson's ratio $v_{\rm S}=0.3$. Fig. 9a shows the FE model of the specimen, where the global distinction between the use of solid and shell elements is made. The FE mesh consisting of solid elements in the lower end of the crossbeam-to-stiffener weld is shown in Figs. 9b and 9c. 8-node brick element with reduced integration (C3D8R) and 8-node quadratic shell element with reduced integration (S8R) are used at and near crossbeam I, and crossbeams II and III, respectively.

A fillet weld with an effective weld throat thickness of 5.00 mm is modelled. A "seam", see Fig. 9c, that duplicates the overlapping nodes along the selected region [37] is applied at the interface between the

[&]quot;*" indicates the cases in which strengthening plates are used.

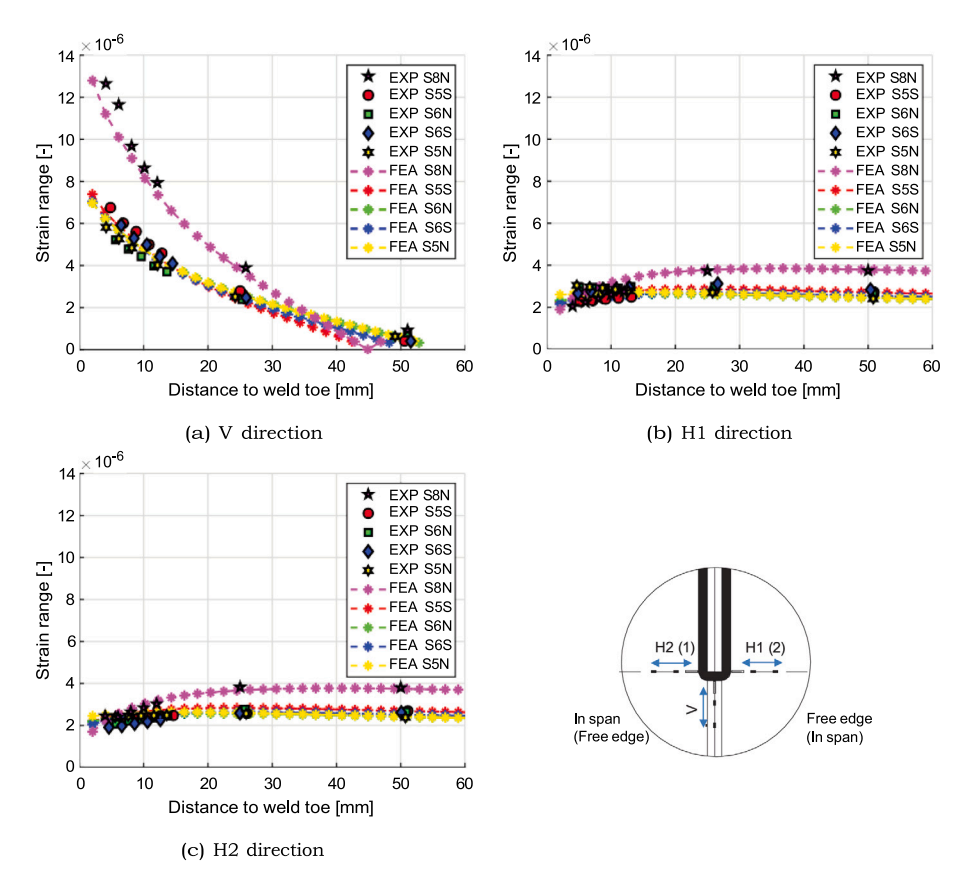
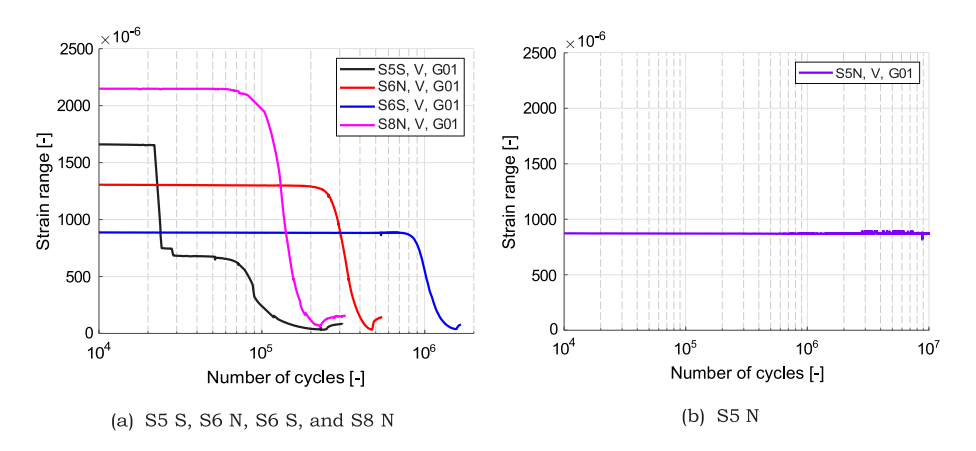


Fig. 10. Comparison of the EXP and FEA results in LC B under the load range of 2×1 kN.



 $\textbf{Fig. 11.} \ \ \textbf{Strain range versus loading cycles from the strain gauge "Stiffener V G01"}.$

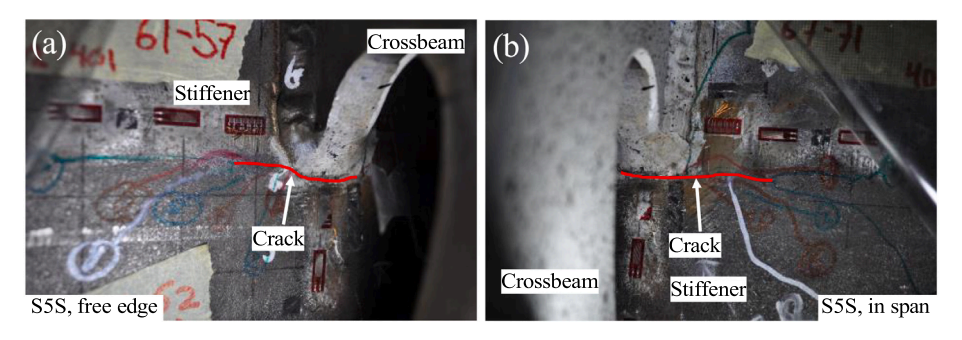


Fig. 12. Fatigue cracks of S5 S after 0.31 million cycles of loading in LC B, 2×250 kN load range.

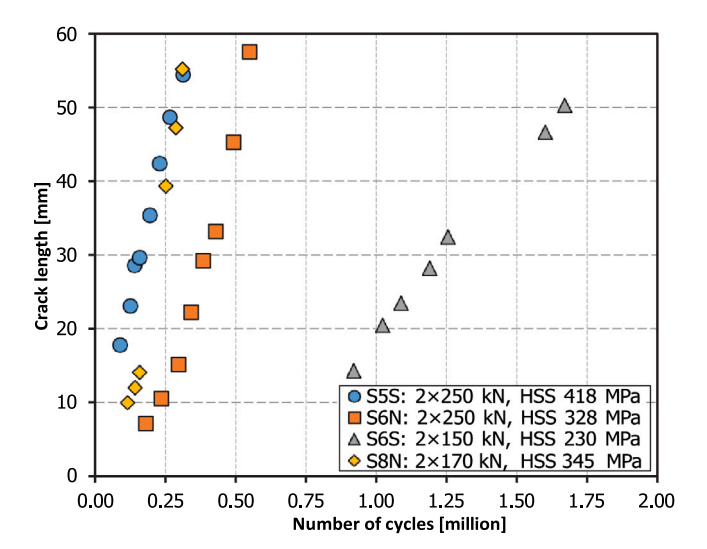


Fig. 13. Crack length versus number of cycles.

crossbeam web and stiffener. The mesh close to the studied details is refined with an element size of approximately 2 mm \times 2 mm \times 2 mm. The element size gradually increases to approximately 50 mm \times 50 mm \times 50 mm and 100 mm \times 100 mm \times 100 mm for the parts meshed with element types C3D8R and S8R, respectively. "Tie" constraints [37] link the brick and shell element parts, see the position of the red rectangle in Fig. 8 and the corresponding interface in Fig. 9a. The ties are applied in all directions. The nodes of a "tie" constrained interface have the same displacements and rotations.

3.5. Validation of the FE calculation

The strain ranges measured from the experiments (EXP) and calculated by the FEA are normalized by a load level of 2×1 kN. The results are presented in Fig. 10. A good agreement is found between the FEA and the EXP in LC B. The stress calculated by FEA is used in Section 4 for fatigue resistance analysis.

3.6. Fatigue crack inspection

Stable strain range distributions are observed under the constant amplitude loading at the initial stage. After a certain number of cycles,

deviations in the strain ranges are observed, caused by the local stiffness deviation due to the development of a fatigue crack. This deviation of the strain range is first observed at the locations 4 mm from the lower end of the weld toe (G01 in V direction). Fig. 11 shows the loading history of the strain ranges at "V G01" in four stiffeners. Note that the first two sharp drops in S5 S, at 2.1×10^4 cycles and at 2.8×10^4 , which may be attributed to "the settling of the specimen/measurements". The strain gauge is checked and works properly afterwards. The reference value of the strain range deviation for S5 S is set after these two drops. S5 N has stable strain ranges till the end of loading. It indicates a runout without fatigue crack detected. Fig. 12 shows a fatigue crack of S5 S after 0.31 million cycles of loading in LC B. The crack initiates at the lower end of the weld in the stiffener, and it then propagates towards the free edge and in span sides of the stiffener.

Fig. 13 gives an overview of the crack propagation of the observed four fatigue cracks. The cracks grow approximately linearly with the number of cycles for crack lengths between the length at first detection of 7 mm to 18 mm and the end of experiments with final crack lengths between 50 mm to 57 mm. The visible crack in S6 S is observed later and grows at a lower rate as compared to the other results. This agrees with the difference in strain ranges in Fig. 7. Fig. 14 shows the marks of the crack edges as measured during the experiments using a clipper with naked eye inspections. The mark numbers in Fig. 13 correspond to the sequential dots in Fig. 14. For S8 N, Fig. 13 shows the longest of the two detected cracks. The cracks are first observed at the lower end of the weld toe, with some shift to the in span side for S6 N and S6 S.

Table 3 gives the numerical values of load ranges, HSS, fatigue lives, and final crack lengths. In line with other fatigue studies of OBDs [1,6,38], the fatigue criteria used in this paper are designated as:

- N₁: Number of cycles corresponding to a 10% strain range deviation observed at 4 mm from the lower end of the weld toe.
- N₂: Number of cycles corresponding to a 25% strain range deviation observed at 4 mm from the lower end of the weld toe.
- N₃: Number of cycles corresponding to the First Visible Crack (FVC) observed by the naked eye.
- N₄: Number of cycles corresponding to an approximately 25 mm long surface crack.
- N_5 : Number of cycles corresponding to an approximately 50 mm long surface crack.

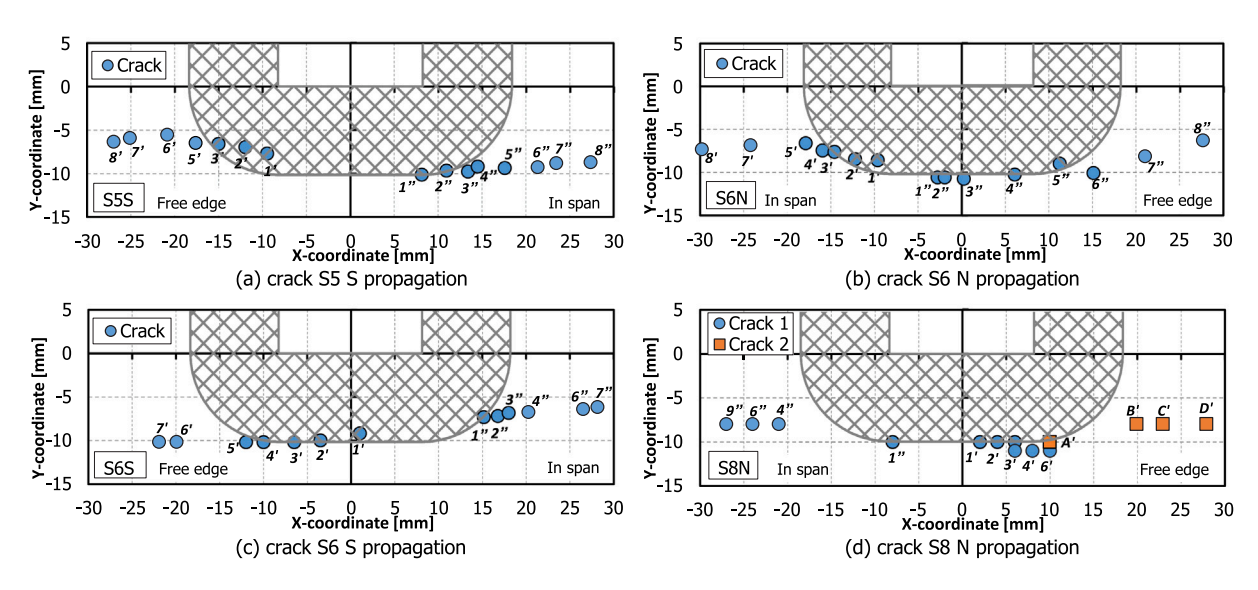


Fig. 14. Patterns of crack propagation (grey hatched area represents the weld leg).

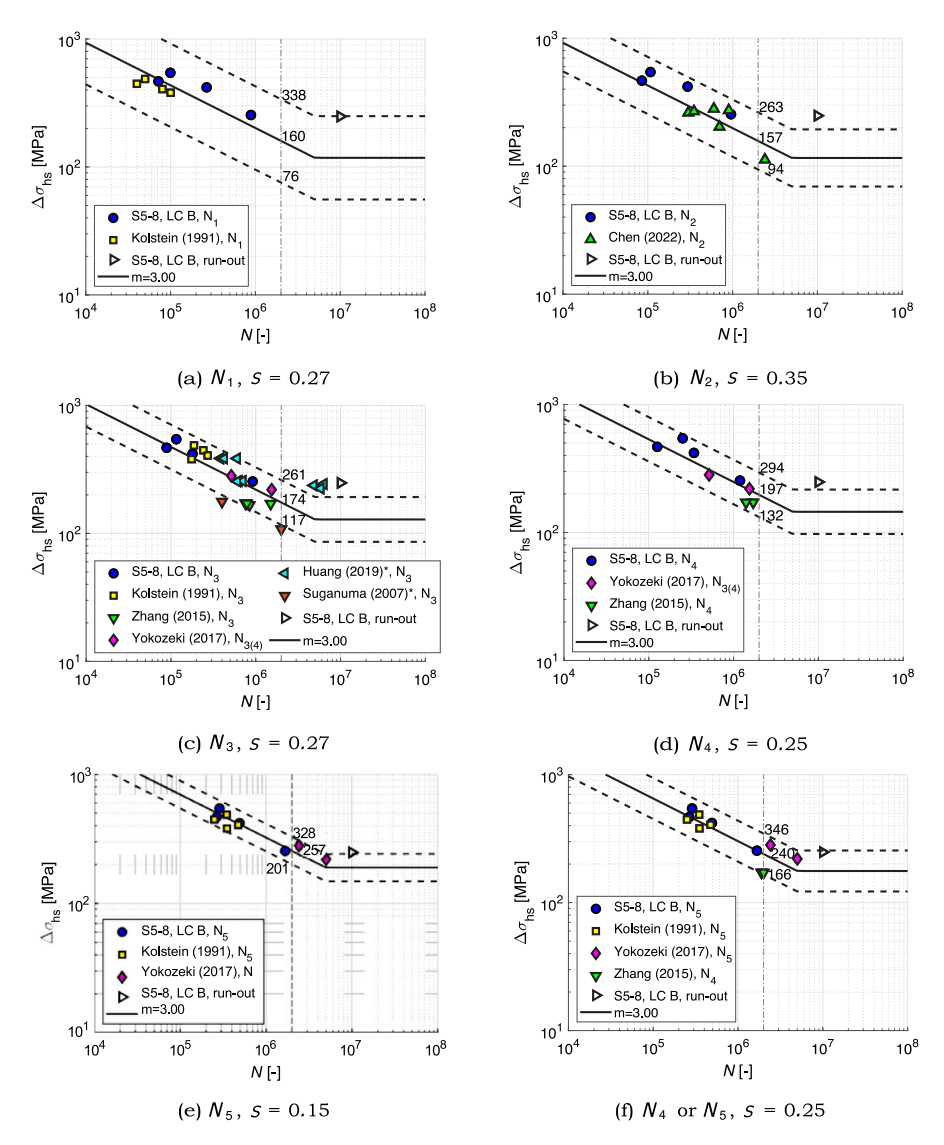


Fig. 15. Statistical analysis of detail C3a using the authors' own experiments and data in the literature [1,11-15] (results with mark "*" are excluded from the statistical analysis).

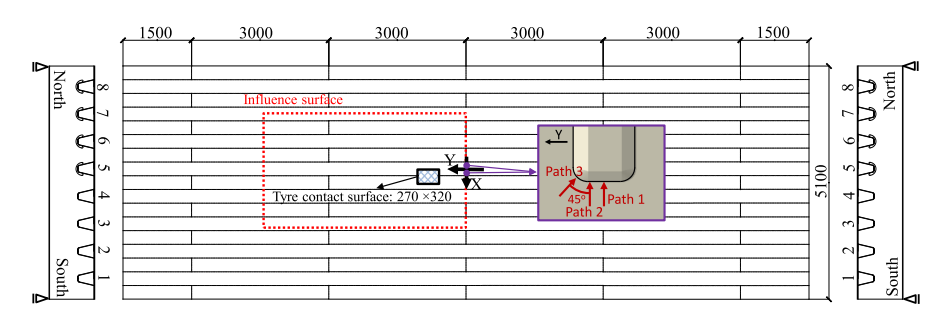


Fig. 16. Overview of the FE model for the influence surface of S5 S and S5 N (unit: mm).

Table 3 Experimental results of tested details using the criteria from N_1 to the termination of experiments in LC B.

Position	ΔP [kN]	$\Delta\sigma_{ m hs}$ [MPa]	N_1	N_2	N_3	N_4	N_5	Experiment terminated cycles	Final crack length [mm]
S5 S	2×250	466	71 743	85 076	88 900	126 000	266 000	313 569	55
S6 N	2×250	418	265 822	294 173	179918	341 000	492 000	548 912	57
S6 S	2×150	254	885 473	956 493	920 353	1190606	1670000	1 670 000	50
S5 N	2×150	248	×	×	×	×	×	10 000 001	×
S8 N	2×170	544	99 362	107 462	115739	251 119	286 810	327 702	56

4. Fatigue resistance

This section presents the evaluation of the fatigue resistances of detail C3a according to [7] using the authors' own experiments and data in the literature. The HSS range used in the experiments from the literature is defined either by measurements or by validated FE models. It means that the results of the FE models used in the HSS assessment agree well with the reported measurements. $\Delta \sigma_{\rm hs}$ is calculated following the TS methodology [7] using the values of FEA . The fatigue criteria N_1 to N_5 introduced in Section 3.6 are used as five possible criteria for fatigue evaluation.

Fig. 15 provides the experimental results in S-N diagrams. The lines in the diagrams represent the survival probabilities 5%, 50%, 95% following the Basquin relation with a fixed slope m = 3, where the statistical procedure of Annex D of EN 1990 is applied [16,18]. In all cases, a constant amplitude fatigue limit, $N_{\rm D}$, is defined at 5×10^6 cycles. From Fig. 15a to Fig. 15f, one of the five criteria is presented in each. Note that the criteria designation used in the references is adjusted to match the criteria given in Section 3.6. Moreover, not all criteria are reported for all experiments in the literature. N_4 is used for [13] in Fig. 15f as N_5 is not available. The failure criteria N_1 and N_2 lead to $\Delta\sigma_{\rm C}$ of 76 MPa and 94 MPa, respectively. The failure criterion N_3 leads to $\Delta \sigma_{\rm C}$ of 117 MPa with a standard deviation of s=0.27. A clear bias is demonstrated between the experiments of [12] and the other experiments. This is because the magnetic particle method, instead of visual control (the naked eye inspection), was used for crack detection in [12]. In [14], progressively increased load levels with an interval of 0.5 million cycles were applied and the visibility of crack at the initiation stage was not reported. The data in these two references are excluded from the statistical analysis. As the standard deviations of the experiments for the other criteria are smaller, the standard deviation of N_3 is attributed to differences in inspection regime. The bias between series for the other criteria is limited and the standard deviations of log(N) are in line with those of other welded details [39], despite the large differences in specimen geometry. This demonstrates that the HSS is rather independent of geometry and therefore appropriate as a basis for the design of this detail. $\Delta \sigma_{\rm C}$ is rounded down to the nearest standardized value of 112 MPa.

The relatively large difference between the failure criteria N_3 and N_5 demonstrates the relative slow crack growth of the detail. The authors consider the failure criterion N_5 , with an approximate surface crack length of 50 mm, appropriate for the assessment of existing structures because it corresponds to a reasonable probability of the detection of surface cracks with the naked eye [40]. The corresponding $\Delta\sigma_{\rm C}$ is rounded down to the nearest standardized value of 160 MPa. This relatively high resistance implies that most existing bridge decks will pass the assessment of this detail.

5. Influence surface of HSS

The HSS in OBDs depends not only on the load level, but also on the position of loads (i.e. tyres of heavy vehicles) and on the support of the structure. The load application and specimen supports applied in the experiments deviate from actual OBDs, in order to simplify the experimental set-ups. This section examines the HSS with more realistic boundary conditions of crossbeams and loading positions by the FE method. In practice, crossbeams are connected to main girders, contrary to the fully supported crossbeams investigated in Section 3.

The simplified FE simulations are therefore carried out with the crossbeams simply supported at their edges. The component dimensions are equal to those of Section 3.4. 20-node brick element with reduced integration (C3D20R) is also commonly used in Abaqus [37]. Element type C3D20R obtains higher strains than the same number of element using type C3D8R, see Appendix. A more realistic fatigue verification with higher stress caused by the wheel loading is carried out in this section using C3D20R. The overall dimensions are adapted as shown in

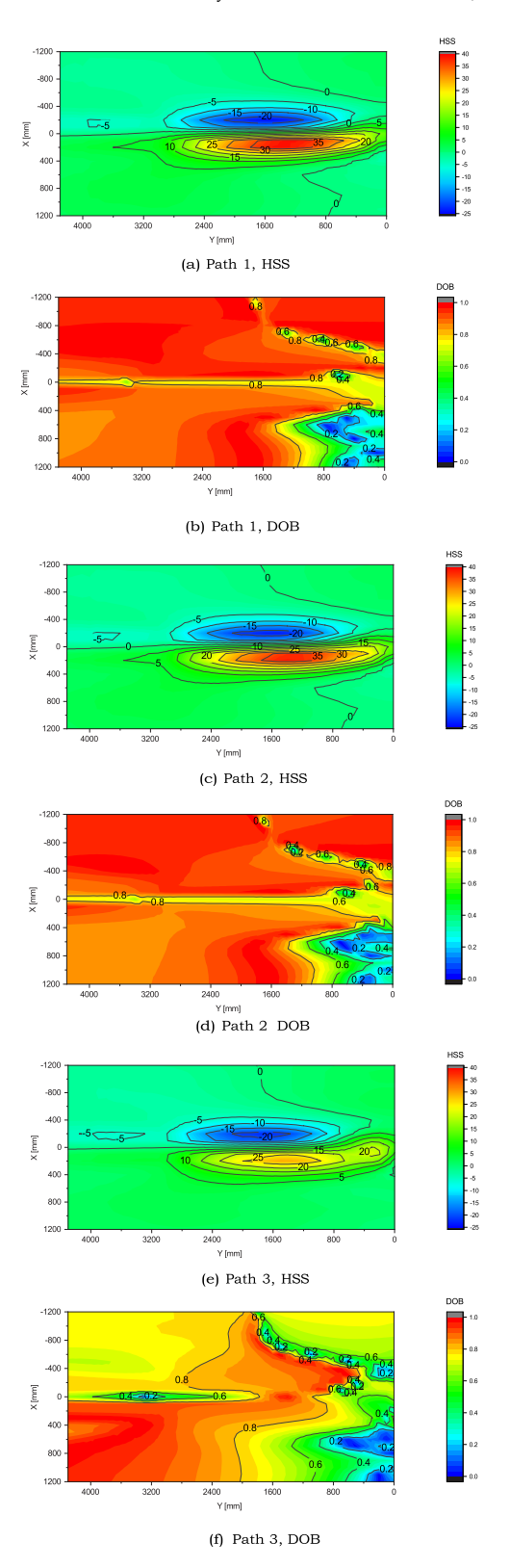


Fig. 17. Influence surface of the HSS and DOB at the S5 S connection.

Fig. 16. The red box indicates the region applied tyre loading. The tyre contact surface is equal to that of a super single tyre in Fatigue Load Model 4 of EN1991-2 [36], i.e., 270 mm in the transverse direction and 320 mm in the running direction. The applied load is equal to the maximum tyre load of super single axles in the same fatigue load model, i.e., 45 kN. The HSS of the critical location, S5 S at Y=0, is

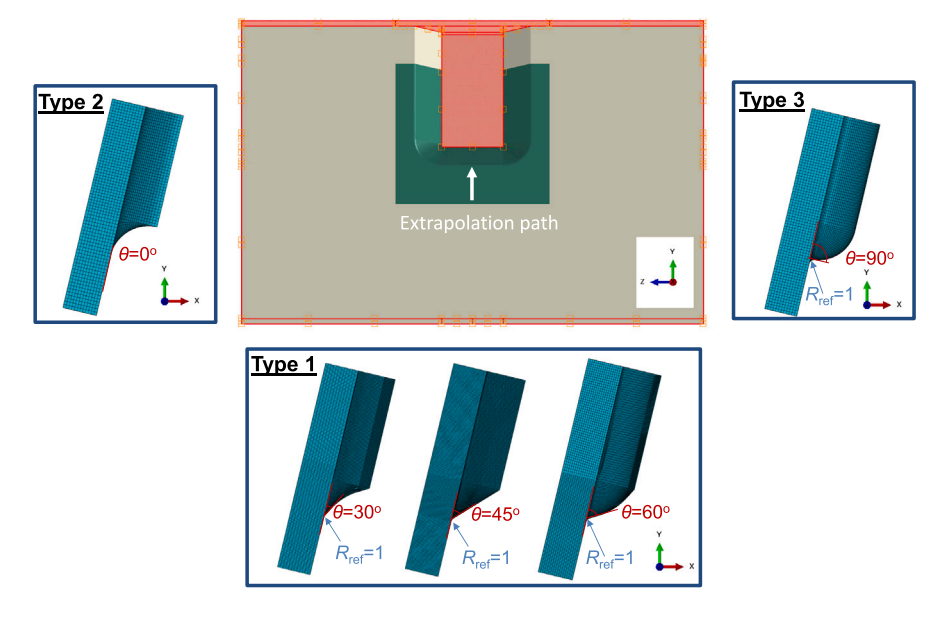


Fig. 18. Overview of the sub-model used for the ENS (unit: mm).

extracted from Path 1, Path 2, and Path 3. The degree of bending (DOB) [41] is calculated using Eq. (2) where σ_b and σ_m are the bending and membrane stresses at the weld toe cross-section, respectively.

$$DOB = \sigma_{\rm h}/(\sigma_{\rm h} + \sigma_{\rm m}) \tag{2}$$

Fig. 17 shows the resulting influence surface of HSS and DOB at the previously mentioned three paths. Path 1 and Path 2 show similar results in HSS and DOB, while Path 3 gives smaller HSS. The largest absolute values of HSS are created for a load centred between approximately Y = 800 mm to 2000 mm, and X = -300 mm to -100 mm. The tensile or compressive stress occurs depending on which side of web the loading is applied on, either S5 S or S5 N. Hence, the largest stress ranges occur if subsequent vehicles (or axles) have a different transverse location on the bridge deck. The DOB is high, >0.8, when $\sigma_{\rm hs}>30$ MPa or <-15 MPa. This agrees with the DOB in the experiments of Section 3.

The maximum HSS range from this study is approximately 63 MPa. In (pr)EN1993-1-9 [16,17], the fatigue resistance curve for such a detail has a slope of m=5 for stress ranges lower than the constant amplitude limit, which is assumed at a number of cycles equal to $N_{\rm D}=5\times10^6$. A cut-off limit $N_{\rm L}=10^8$ is designated below which the stress ranges of a variable-amplitude calculating do not contribute to fatigue damage.

The fatigue resistances $\Delta\sigma_C$ of 112 MPa and 160 MPa obtained in Section 4 have constant amplitude fatigue limits $\Delta\sigma_D$ 83 MPa and 118 MPa and cut-off stresses $\Delta\sigma_L$ of 45 MPa and 65 MPa, respectively. The maximum HSS range in the considered deck is hence lower than the cut-off stress range proposed for the assessment of existing bridge decks, and it is in between the constant amplitude fatigue limit and the cut-off stress range for new bridge decks. This implies that the considered deck will pass the assessment for detail C3a, and it will also be sufficient for most designs. Only in the case of very heavily loaded bridges, a stronger deck might be required for detail C3a.

6. ENS assessment of fatigue resistance

A weld flank angle of $\theta=45^{\rm o}$ is used in the simulations of Section 3. In practice, θ depends on the welding procedure. For instance, overhead welding may result in a convex weld profile. The HSS is insensitive to the local weld geometry such as the flank angle. However, it is known that the flank angle can influence fatigue resistance [17]. Therefore, the influence of the weld flank angle is examined by the ENS. The sub-modelling method available in Abaqus [37] bridges the difference

in scale between the local weld geometry (sub-model) and overall specimen geometry (global model). The overall specimen geometry is the same as that of Section 3.4. The displacements of sub-model are constrained to match the displacements of global model at the intersections. IIW recommends a notch radius of $R_{\rm ref}=1$ mm and local refined mesh at the studied locations [21]. Both recommendations are applied here.

Element type C3D20R is used in the sub-models. The outer (grey) and inner (green) parts have element sizes of approximately 0.5 mm \times 0.5 mm \times 0.5 mm and 0.2 mm \times 0.2 mm \times 0.2 mm, respectively. Fig. 18 shows the sub-models with three types of weld profiles. "Tie" constraints link the two parts [37]. The highlighted surfaces of outer part are driven by the global model, as shown in Fig. 8. Type 1 represents the weld profiles with $\theta = 30^{\circ}$, 45°, and 60°, which are all within the requirements of prEN1993-1-9 [17]. Types 2 and 3 represent the extreme cases with $\theta = 0^{\circ}$ and 90° , respectively. Type 2 represents a post-weld grind treatment [2,12], whereas Type 3 is considered to study the potentially detrimental effect of a large flank angle, which might be a consequence of the limited space at the lower end of the weld. Note that the element size in the Type 2 detail model is larger than the other two types. This is assumed not to affect the analysis as the transition between the weld and base metal is smooth, resulting in smaller stress concentrations.

Fig. 19 shows the principal and von Mises equivalent stresses under $2\times 1\,$ kN. The maximum principal stress criterion is more suitable than the von Mises stress criterion for proportional loading [42]. Both criteria are presented for comparison. The maximum stress in the Type 2 detail is predicated on the weld profile with a small shift to the free edge side. The models of Type 1 and Type 3 details predict the maximum stresses in the transition region, at the corner of the lower end of the weld on the free edge side. Interestingly, the Type 1 detail predicts a higher maximum stress for the $\theta=45^{\circ}$ flank angle than the other flank angles of $\theta=30^{\circ}$ and 60° . This is attributed to a complex interaction between the loaded stiffener and crossbeam web. It is also observed that the HSS (explained in the last paragraph of this section) calculated from the sub-models is affected by θ . The Type 3 detail model predicts a higher maximum stress than the other two .

A scale factor, $K_{\rm en}$, is calculated using Eq. (3) [28]. Either maximum principal or von Mises equivalent stress is used for $\sigma_{\rm en}$. $K_{\rm en}$ is, therefore, calculated using the HSS from the sub-models. The HSS is extrapolated following the white arrow direction in Fig. 18.

$$K_{\rm en} = \sigma_{\rm en}/\sigma_{\rm hs} \tag{3}$$

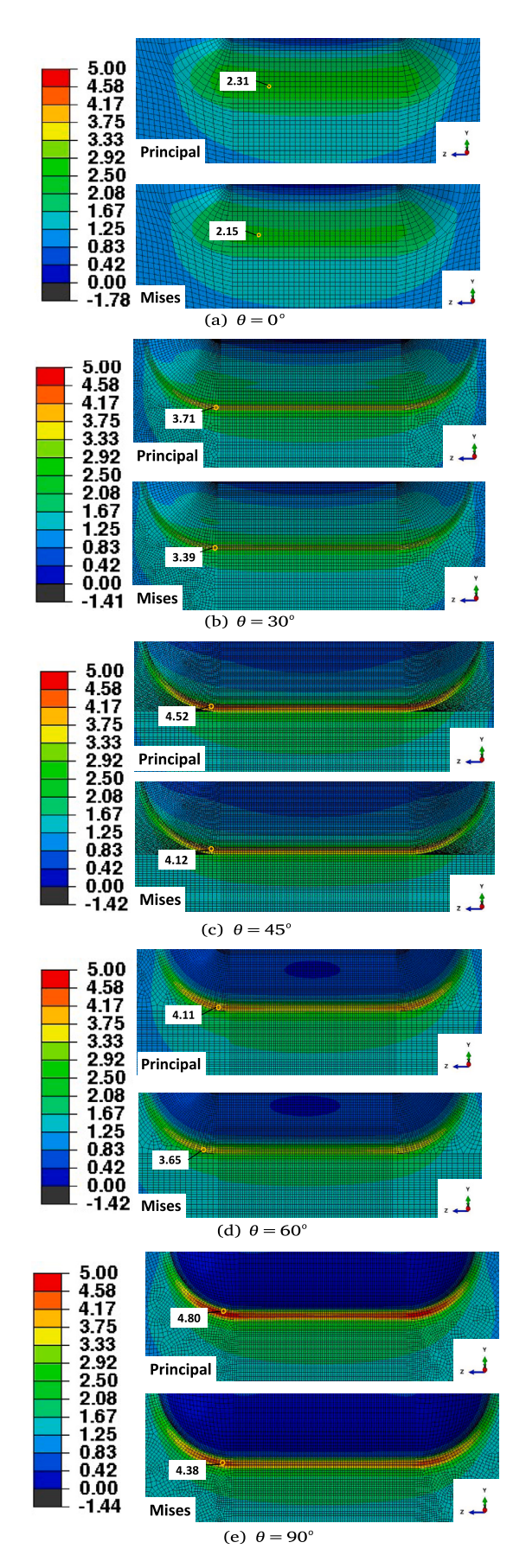


Fig. 19. The ENS of detail C3a with θ under the load of 2×1 kN (unit: MPa).

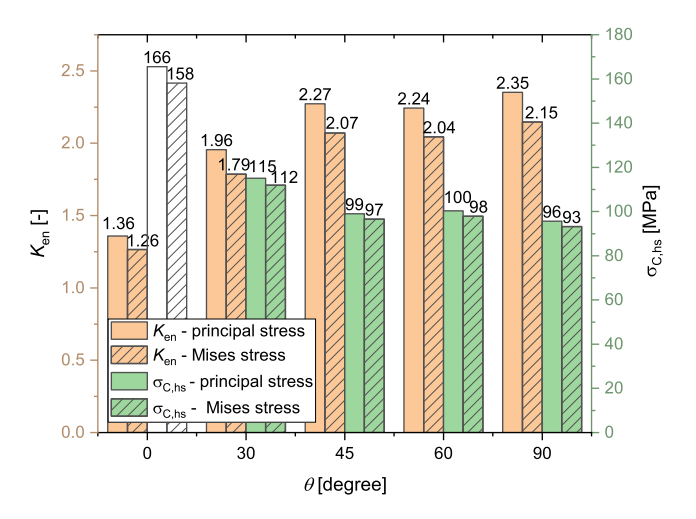


Fig. 20. $K_{\rm en}$ and $\Delta\sigma_{\rm C.hs}$ versus θ .

The predicted fatigue resistance of HSS, $\Delta\sigma_{\rm C,hs}$, can be obtained using the characteristic values of ENS, $\Delta\sigma_{\rm C,en}$, as shown in Eq. (4) with 225 MPa and 200 MPa for the principal stress and von Mises equivalent stress criteria [17], respectively.

$$\Delta\sigma_{\rm C,hs} = \Delta\sigma_{\rm C,en}/K_{\rm en} \tag{4}$$

Fig. 20 compares the predicted $\Delta\sigma_{\rm C,hs}$ with θ . As $R_{\rm ref}$ is not available for $\theta=0^{\rm o}$ (Type 2) model, the values 166 MPa and 158 MPa are presented in hollow columns for comparison only.

The scale factor $K_{\rm en}$ increases with θ in the range of $0^{\rm o}$ to $45^{\rm o}$ and afterwards keeps constant till $\theta=90^{\rm o}$. The von Mises equivalent stress criterion gives a lower $K_{\rm en}$ and $\Delta\sigma_{\rm C,hs}$ predictions than the principal stress criterion. The $\Delta\sigma_{\rm C,hs}$ based on the ENS ranges from 97 MPa to 115 MPa in the Type 1 detail, close to the statistical analysis obtained values 94 MPa and 117 MPa in Section 4 using the failure criteria N_2 and N_3 , respectively. Only 3% to 4% lower fatigue resistance results for $\theta=90^{\rm o}$ compared with the $\theta=45^{\rm o}$ case. This finding is close to the fracture mechanics predictions in [43] for the weld toe cracking in stiffener-to-deck welds between crossbeams, where a 2% reduction is obtained between the same two flank angles. The results imply that, compared to the standard flank angle of $\theta=45^{\rm o}$, a higher fatigue resistance is obtained for a smaller angle, whereas a larger angle gives no significant reduction in the resistance.

7. Conclusions

Examination of the fatigue behaviour of the lower end of the weld in connections between the crossbeam and stiffener with cut-outs in orthotropic bridge decks is presented in this paper. This construction detail was included by neither in the first nor in second generation of (pr)EN1993-1-9 [16,17]. Eight independent experiments are tested in fatigue using one full-scale specimen. The fatigue resistances are determined based on the experiments in the current paper and 27 other experiments in the literature. The study has led to the following conclusions and recommendations:

- The bias in the fatigue resistance between different series is small for most evaluated cases, despite the significantly different specimen geometries applied in different series. This confirms that the HSS can be used as the basis for evaluating the fatigue resistance of the detail of study for a wide range of geometries.
- Relative slow crack growth is observed for this detail, which is attributed to the cracks growing away from the weld, e.g. towards a region with a smaller stress-raising effect. This implies that the fatigue resistance depends significantly on the criterion used for evaluation. This study evaluates the fatigue resistance for the

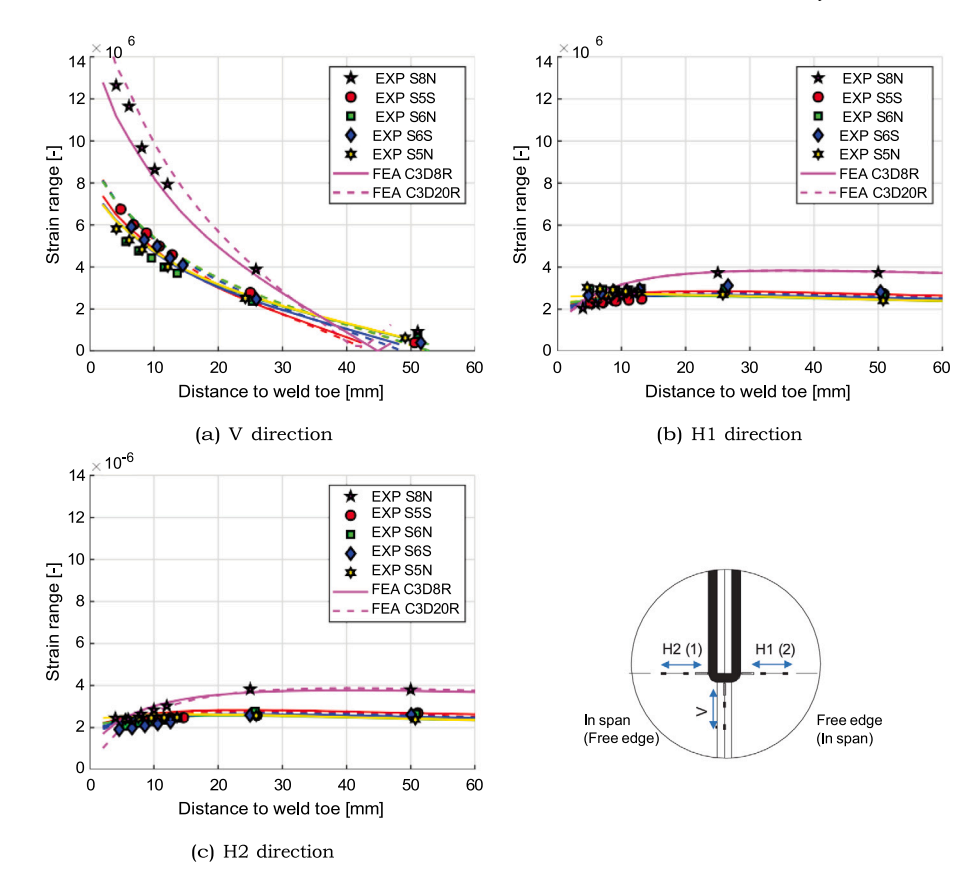


Fig. A.1. Strain distribution from the experiments and FE calculations using C3D8R or C3D20R in LC B under the load range of 2×1 kN.

criteria ranging between the first deviation of strain ranges measured by strain gauges to a surface crack length of approximately 50 mm. The corresponding characteristic fatigue resistance values of HSS, defined as the 95% survival limit at 2 million cycles, range between 76 and 166 MPa, respectively.

- For the design of new bridge decks, the authors consider a crack that is first visually observed as a proper evaluation criterion for fatigue resistance, as a balance between full structural integrity (not compromising the load-bearing resistance) and relatively high fatigue resistance (allowing for relatively low-weight components). The associated fatigue resistance is 112 MPa (roundeddown value), resulting from the 14 available experiments for this criterion. This resistance is proposed for (and already adopted in) the Technical Specification TS 1993-1-901 [7].
- An additional S-N curve is proposed for assessing existing bridge decks. The authors consider a surface crack with an approximate length of 50 mm appropriate as a criterion for this case because it corresponds with a reasonable probability of the detection of surface cracks with the naked eye [40]. The associated fatigue resistance of 160 MPa resulting from 10 experiments is relatively high. This implies that most existing bridge decks will pass the assessment of this detail.
- In the geometry analysed in this study, the configuration includes 6 mm thick trapezoidal stiffeners with Haibach shape cut-outs and 16 mm thick crossbeams, the maximum hot spot stress range obtained at detail C3a for the highest tyre load of Fatigue Load Mode 4 in EN 1991-2 [36] is approximately 63 MPa. Using the S-N curve format of Eurocodes, the constant amplitude fatigue limit is 83 MPa and the cut-off value is 45 MPa for the proposed design resistance curve. These values do not account for the partial factors. The maximum stress range of Fatigue Load Model 4 is between these values. This implies that a modified geometry than the one studied here might be required for very heavily loaded

- bridge decks, while the design is expected to be sufficient for more common, moderately loaded bridge decks.
- The effect of weld flank angle is studied using the ENS. The ENS with a flank angle $\theta=30^{\circ}$ is approximately 18% smaller than the value with a flank angle $\theta=45^{\circ}$. The ENS is almost equal between $\theta=45^{\circ}$ and 90° . Within the requirements of prEN1993-1-9 [17] ($30^{\circ} \le \theta \le 60^{\circ}$), the effect of weld flank angle on fatigue resistance is hence limited.
- The predicted fatigue resistance for the HSS, as derived from the ENS method, ranges from 97 MPa to 115 MPa. This prediction is close to the statistical analysis of the experimental data at the onset of cracking, which ranges from 94 MPa (for the criterion of 25% drop of strain range at 4 mm distance from the weld toe) to 117 MPa (first visible crack).

CRediT authorship contribution statement

Weijian Wu: Writing – review & editing, Writing – original draft, Visualization, Validation, Software, Methodology, Investigation, Formal analysis, Data curation, Conceptualization. Johan Maljaars: Writing – review & editing, Validation, Supervision, Data curation, Conceptualization. David Malschaert: Writing – review & editing, Validation, Software. Milan Veljkovic: Writing – review & editing, Supervision, Methodology. Henk Kolstein: Writing – review & editing, Supervision, Funding acquisition, Data curation. Richard Pijpers: Writing – review & editing, Validation, Data curation.

Declaration of competing interest

The authors declare that they have no known competing financial interests or personal relationships that could have appeared to influence the work reported in this paper.

Data availability

Data will be made available on request.

Acknowledgements

The experimental study is sponsored by the Dutch bridge asset owner Rijkswaterstaat (RWS). The authors acknowledge Jorrit Rodenburg from TNO for the FEA of some experiments used in the literature. The authors acknowledge Frank van Dooren from RWS for the discussions in the project meetings. The first author would like to thank China Scholarship Council, China for the study funding.

Appendix. Comparison of element types for the detail of study

Fig. A.1 compares the strains computed by the FE models using the element types C3D8R (solid lines) and C3D20R (hash lines) and the measured strains in the experiments. Higher strain ranges are observed with C3D20R. Compared to the measurements, the models with C3D20R over-predict the strain for S8 N, S5 N, and S6 N. The results with C3D8R are used in the statistical analysis as a conservative choice.

References

- M.H. Kolstein, Fatigue Classification of Welded Joints in Orthotropic Steel Bridge Decks (doctoral thesis), Delft University of Technology, 2007.
- [2] R. Connor, J. Fisher, W. Gatti, V. Gopalaratnam, B. Kozy, B. Leshko, D.L. Mc-Quaid, R. Medlock, D. Mertz, T. Murphy, et al., Manual for Design, Construction, and Maintenance of Orthotropic Steel Deck Bridges, American association of state highway and transportation officials, 2012.
- [3] R. Wolchuk, Orthotropic Redecking of Bridges on the North American Continent, Struct. Eng. Int. 2 (2) (1992) 125–130.
- [4] J. Leendertz, Fatigue Behaviour of Closed Stiffener to Crossbeam Connections in Orthotropic Steel Bridge Decks (doctoral thesis), Delft University of Technology, 2008
- [5] AISC, Design Manual for Orthotropic Steel Plate Deck Bridges, 1963, pp. 1–237.
- [6] W. Wu, M. Veljkovic, H. Kolstein, R. Pijpers, J. Maljaars, Fatigue behaviour of root crack in stiffener-to-deck plate weld at crossbeam of orthotropic bridge decks, Eng. Struct. 306 (2024) 117710.
- [7] prT.S. 1993-1-901, Fatigue Design of Orthotropic Bridge Decks with the Hot Spot Stress Method (final draft), European Committee for Standardization, 2023.
- [8] C. Miki, T. Konishi, Retrofit Engineering for Steel Bridge Structures in Japan, in: IABSE Symposium, Weimar, 2007.
- [9] R.J. Dexter, J.W. Fisher, Fatigue Cracking of Orthotropic Steel Decks, Tech. Rep., IABSE reports, Zurich, 1997.
- [10] J. Di, X. Ruan, X. Zhou, J. Wang, X. Peng, Fatigue assessment of orthotropic steel bridge decks based on strain monitoring data, Eng. Struct. 228 (2021) 111437.
- [11] K. Yokozeki, High Fatigue Resistant Orthotropic Steel Bridge Decks (doctoral thesis). (July) Tokyo City University, Tokyo, 2017.
- [12] H. Suganuma, C. Miki, Full Size Fatigue Tests of the New Orthotropic Steel Deck System, Tech. Rep, Japan Institute of Welding, Tokyo, 2007.
- [13] Q.-H. Zhang, C. Cui, Y.-Z. Bu, Y.-M. Liu, H.-W. Ye, Fatigue tests and fatigue assessment approaches for rib-to-diaphragm in steel orthotropic decks, J. Constr. Steel Res. 114 (2015) 110–118.
- [14] Y. Huang, Q. Zhang, Y. Bao, Y. Bu, Fatigue assessment of longitudinal rib-to-crossbeam welded joints in orthotropic steel bridge decks, J. Constr. Steel Res. 159 (2019) 53–66.
- [15] J. Chen, C. Wei, Y. Zhao, Fatigue resistance of orthotropic steel deck system with double-side welded rib-to-deck joint, Adv. Struct. Eng. (2022).
- [16] EN1993-1-9, Eurocode 3: Design of Steel Structures Part 1-9: Fatigue, European Committee for Standardization, 2005.

- [17] prEN 1993-1-9, Eurocode 3: Design of Steel Structures Part 1-9: Fatigue. Doc N3751 (enquiry draft) Committee for Standardization, 2023.
- [18] H. Bartsch, K. Drebenstedt, B. Seyfried, M. Feldmann, U. Kuhlmann, T. Ummenhofer, Analysis of fatigue test data to reassess EN 1993-1-9 detail categories, Steel Constr. 13 (4) (2020) 280–293.
- [19] AASHTO, AASHTO LRFD Bridge Design Specifications, ninth ed., American Association of State Highway and Transportation Officials, 2020.
- [20] JSSC, Fatigue Design Recommendations for Steel Structures, Japanese Society of Steel Construction, 2012.
- [21] A.F. Hobbacher, Recommendations for Fatigue Design of Welded Joints and Components, in: C. Mayer (Ed.), second ed., in: IIW Collection, Springer International Publishing, 2016.
- [22] DNVGL-RP-C203, Recommended Practice Fatigue Design of Offshore Steel Structures, Edition April 2016, DNV (DNVGL).
- [23] P. Dong, A structural stress definition and numerical implementation for fatigue analysis of welded joints, Int. J. Fatigue 23 (10) (2001) 865–876.
- [24] S. Pandit, Finite Element Modelling of Open Longitudinal Stiffener to Crossbeam Connection in OSD Bridges for Hot-Spot Stress Determination (master's thesis), Delft University of Technology, 2020.
- [25] D. van der Ende, Finite Element Analysis of the Closed Stiffener to Crossbeam Connection in OSDs Using the Hot Spot Stress Approach (master's thesis), Delft University of Technology, 2020.
- [26] J.D. Rodenburg, Sjoerd, T. Hengeveld, Bas, M.M. Wijnbeld, J. Maljaars, Generic method of local thickening in shell element FEM models for orthotropic bridge decks, ce/papers 6 (3–4) (2023) 2540–2545.
- [27] P. Lazzarin, P. Livieri, Notch stress intensity factors and fatigue strength of aluminium and steel welded joints, Int. J. Fatigue 23 (3) (2001) 225–232.
- [28] D. Radaj, C.M. Sonsino, W. Fricke, Fatigue Assessment of Welded Joints by Local Approaches: Second Edition, Elsevier Ltd, 2006.
- [29] J. Maljaars, R. Pijpers, W. Wu, H. Kolstein, Fatigue resistance of rib to deck, crossbeam to deck and deck to deck welds in orthotropic decks using structural stress, Int. J. Fatigue 175 (2023) 107742.
- [30] W. Wu, M. Veljkovic, H. Kolstein, J. Maljaars, R. Pijpers, Fatigue behaviour of toe and root stiffener cracks in stiffener-to-deck plate weld of orthotropic bridge decks, Eng. Struct. 305 (2024) 117740.
- [31] F.R. Mashiri, X.-L. Zhao, Thickness Effect in Welded Joints-A Review, International Society of Offshore and Polar Engineers, Seoul, 2005.
- [32] BSI 7910, BSI Standards Publication Guide to methods for assessing the acceptability of flaws in metallic structures, British Standards Institution (2015).
- [33] T.R. Gurney, Thickness Effect in 'Relatively Thin' Welded Joints, Tech. Rep., Welding Inst., Cambridge, 1995.
- [34] EN10025-2, Hot Rolled Products of Structural Steels. Part 2: Technical Delivery Conditions for Non-Alloy Structural Steels, European Committee for Standardization, 2004.
- [35] ISO 5817, Welding-Fusion-welded joints in steel, nickel, titanium and their alloys (beam welding excluded)-Quality levels for imperfections, 2014.
- [36] EN1991-2, EN 1991: Actions on structures—Part 2: Traffic loads on bridges, European Committee for Standardization, 2003.
- [37] Simulia, Abaqus User's Manual version 2019, Dassault Systèmes Simulia Corp., Providence, RI, USA, 2019.
- [38] F.B.P. De Jong, Renovation Techniques for Fatigue Cracked Orthotropic Orthotropic Steel Bridge Decks (doctoral thesis), Delft University of Technology, 2006.
- [39] BS 7608:2014+A1:2015, Guide to fatigue design and assessment of steel products, British Standards Institution, 2014.
- [40] J. Maljaars, A.C. Vrouwenvelder, Probabilistic fatigue life updating accounting for inspections of multiple critical locations, Int. J. Fatigue 68 (2014) 24–37.
- [41] E. Niemi, W. Fricke, S.J. Maddox, Structural Hot-Spot Stress Approach to Fatigue Analysis of Welded Components, second ed., in: IIW Collection, Springer, 2018.
- [42] M. Bäckström, G. Marquis, A review of multiaxial fatigue of weldments: Experimental results, design code and critical plane approaches, Fatigue Fract. Eng. Mater. Struct. 24 (5) (2001) 279–291.
- [43] W. Wu, H. Kolstein, M. Veljkovic, Fatigue resistance of rib-to-deck welded joint in OSDs, analyzed by fracture mechanics, J. Constr. Steel Res. 162 (2019).